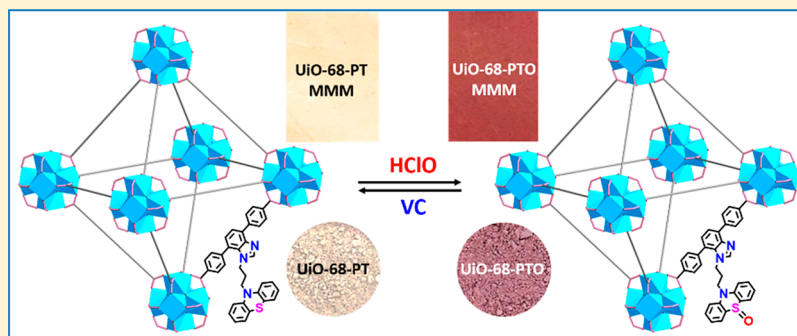


UiO-68-PT MOF-Based Sensor and Its Mixed Matrix Membrane for Detection of HClO in Water

Qian-Ying Li, Yan-An Li,*^{ORCID} Qun Guan,^{ORCID} Wen-Yan Li, Xiao-Jie Dong, and Yu-Bin Dong*^{ORCID}

College of Chemistry, Chemical Engineering and Materials Science, Collaborative Innovation Center of Functionalized Probes for Chemical Imaging in Universities of Shandong, Key Laboratory of Molecular and Nano Probes, Ministry of Education, Shandong Normal University, Jinan 250014, P. R. China

Supporting Information



ABSTRACT: As an important type of reactive oxygen species (ROS), hypochloric acid (HClO) is closely linked with our daily life, and its convenient and rapid detection is very significant and imperative. Fluorescent and visual probes are being recognized as powerful and convenient tools for detection of ROS in the environment and living organisms by visualizing and imaging. In this contribution, a new metal–organic framework-based fluorescent probe **UiO-68-PT**, which was generated from a phenothiazine-decorated benzimidazole bridging dicarboxyl ligand and $ZrCl_4$ under solvothermal conditions via in situ one-pot approach, is reported. The obtained **UiO-68-PT** features a unique HClO and Vitamin C-triggered reversible redox process, which is accompanied by both visual and fluorescence changes. Therefore, it can be a highly sensitive, specific, and reusable sensor to detect HClO species in water via both visual and fluorogenic observation (turn-on). Furthermore, its mixed membrane material (MMM) was fabricated by the combination of **UiO-68-PT** and poly(vinyl alcohol), and the obtained hydrophilic MMM can be used as a reversible colorimetric card for visual detection of the HClO in aqueous solution.

INTRODUCTION

As a very important type of reactive oxygen species (ROS), hypochloric acid (HClO) plays a vital role in our daily life and innate immune system of the living organism. For example, HClO ranging from 1×10^{-5} to 1×10^{-2} M is extensively used for antimicrobial treatment of tap water.¹ On the one hand, in vivo, HClO, which is produced from H_2O_2 and chloride ions catalyzed by myeloperoxidase (MPO), acts as an intracellular regulator and can activate cell differentiation, proliferation, and the immune system during physiological and pathological processes.² On the other hand, excessive HClO could oxidize nucleic acids, proteins, cholesterol, lipids, and so on, consequently leading to tissue damage and causing various diseases such as angiocardopathy, lung injury, osteoarthritis, atherosclerosis, and even cancer.³ Therefore, the development of efficient and convenient methods for detecting HClO is very significant and urgently required.

Fluorescent probe-based method has been recognized as a powerful tool to detect small molecular species such as HClO due to their highly sensitive, selective, real-time, and easy manipulating nature.^{4–6} For example, Nagano's group,⁷ Ma's

group,⁸ and so on developed a series of HClO-specific fluorescent probes, in which various fluorophores^{9,10} such as rhodamine, boron-dipyrromethene (BODIPY), fluorescein, naphthalimide, and so on were chosen as the fluorescence response groups. All these organic fluorophores, however, make the probes possess advantage in detecting HClO in organic or organic cosolvents over the aqueous solution due to their organic nature. Even dispersed in the cosolvent system, the organic probes are still prone to aggregate; furthermore, they induce the aggregation-caused quenching (ACQ),¹¹ and this will inevitably limit their application in aqueous system such as environmental water monitoring and assessment.

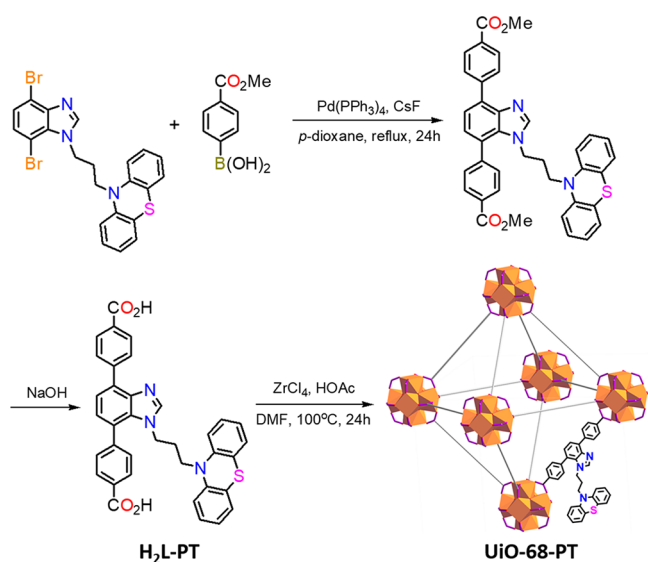
As an important class of porous crystalline hybrid materials, metal–organic frameworks (MOFs) have received enormous attention due to their numerous potential applications.¹² In principle, organic fluorophores could be grafted on MOF frameworks via either in situ one-pot synthesis or postsynthetic modification (PSM). In doing so, the possible ACQ effect

Received: April 9, 2019

should be averted because of their orderly arrangement in MOF frameworks.¹³ Besides, the large surface areas of MOFs could facilitate the contact between the MOF-based probes and the analytes; moreover, their open channels would permit a rapid and uncommitted diffusion of the analytes. Consequently, a fast sensing response could be achieved. Very recently, an attractive approach has been developed for the preparation of MOF-based and polymer-involved mixed matrix membranes (MMMs).¹⁴ This alternative way not only realized the MOF processability but also made the MOF-based shaped devices for the practical applications in water monitoring and treatment possible.

In this contribution, we report a novel UiO-68 type of MOF, namely, **UiO-68-PT**, which was prepared by the combination of the prefunctionalized dicarboxylic acid ligand **H₂L-PT** and Zr(IV) salt under solvothermal conditions (Scheme 1). The

Scheme 1. Synthesis of **H₂L-PT** and **UiO-68-PT**



obtained **UiO-68-PT** with phenothiazine-based moiety is a highly sensitive and selective MOF-based probe for detecting HClO via both visual and fluorogenic ways (turn-on). So far as we know, this is the first reusable MOF-based fluorescent probe for HClO.¹⁵ More importantly, by mixing **UiO-68-PT** with poly(vinyl alcohol) (PVA), a **UiO-68-PT**-based MMM was fabricated, and it can be a reusable colorimetric card to selectively detect the HClO in water.

EXPERIMENTAL SECTION

Synthesis of H₂L-PT. A mixture of 10-(3-(4,7-dibromo-1H-benzo[*d*]imidazol-1-yl)propyl)-10H-phenothiazine (1 mmol, 0.515 g), 4-methoxycarbonylphenylboronic acid (3 mmol, 0.54 g), CsF (4.75 mmol, 0.72 g), and tetrakis(triphenylphosphine) palladium (0.33 mmol, 0.38 g) in anhydrous dioxane (50 mL) was refluxed for 24 h in N₂. After removal of the solvent in vacuum, the crude product was purified by column chromatography (silica gel, CH₂Cl₂/ethyl acetate = 10:1) to afford the esterified ligand as white crystalline solids (0.363 g, yield 58%). IR (KBr pellet cm⁻¹): 3343 (m), 3051 (m), 2944 (m), 1715 (s), 1456 (m), 1375 (s), 1280 (s), 1188 (s), 863 (s), 775 (s), 632 (w). ¹H NMR (400 MHz, deuterated dimethyl sulfoxide (DMSO-*d*₆), 25 °C, tetramethylsilane (TMS), ppm): 8.26 (s, 1H, -CH-), 8.23 (s, 2H, -C₆H₂-), 8.09–8.06 (d, 2H, -C₆H₄-), 8.03–8.01 (d, 2H, -C₆H₄-), 7.63–7.61 (d, 2H, -C₆H₄-), 7.63–7.60 (d, 2H, -C₆H₄-), 7.24–7.22 (t, 2H, -C₆H₄-), 7.14–7.11 (d, 2H, -C₆H₄-), 7.09–7.06 (d, 2H, -C₆H₄-), 6.95–6.93 (t, 2H, -C₆H₄-), 4.08–4.05 (t,

2H, -CH₂-), 3.90 (s, 3H, -CH₃), 3.90 (s, 3H, -CH₃), 3.43–3.40 (t, 2H, -CH₂-), 1.59–1.54 (m, 2H, -CH₂-). Anal. (%) calcd: C 72.94, H 4.99, N 6.72; Found: C 72.81, H 5.07, N 6.64.

The as-synthesized esterified ligand (1 mmol, 0.625 g) was stirred in a tetrahydrofuran (THF) (20 mL)/H₂O (50 mL) solution of NaOH (25 mmol, 1.0 g) at 40 °C for 12 h. After removal of THF in vacuum, the residue was heated, until the solid was fully dissolved; then, the resulting solution was acidified with diluted HCl, until no more precipitate was generated (pH < 2). The formed precipitate was washed with water and dried in air to afford **H₂L-PT** as white solids (0.59 g, yield 98%). IR (KBr pellet cm⁻¹): 2963 (m), 1688 (vs), 1607 (s), 1458 (s), 1424 (m), 1323 (s), 1294 (s), 1184 (s), 1016 (s), 769 (s), 743 (s), 547 (w). ¹H NMR (400 MHz, DMSO-*d*₆, 25 °C, TMS, ppm): 8.19–8.18 (d, 1H, -C₆H₂-), 8.18–8.17 (d, 2H, -C₆H₄-), 8.05–8.04 (d, 2H, -C₆H₄-), 8.04–8.03 (d, 2H, -C₆H₄-), 7.60–7.58 (d, 1H, -C₆H₂-), 7.58–7.56 (d, 2H, -C₆H₄-), 7.24–7.22 (d, 1H, -CH-), 7.13–7.12 (d, 2H, -C₆H₄-), 7.10–7.08 (d, 2H, -C₆H₄-), 6.94–6.90 (t, 2H, -C₆H₄-), 6.63–6.61 (d, 2H, -C₆H₄-), 4.10–4.07 (t, 2H, -CH₂-), 3.44–3.47 (t, 2H, -CH₂-), 1.57–1.54 (m, 2H, -CH₂-). Anal. (%) calcd: C 72.34, H 4.55, N 7.03; Found: C 72.66, H 4.67, N 6.96.

Synthesis of UiO-68-PT. ZrCl₄ (9.6 mg, 0.041 mmol), **H₂L-PT** (15 mg, 0.025 mmol), and acetic acid (120 μL) were dissolved in dimethylformamide (DMF; 3.2 mL) and then filtered into a Pyrex glass tube. The tightly capped flasks were kept in an oven at 100 °C under static conditions for 24 h. The product was isolated by centrifugation and washed with DMF (three times). The obtained powder was immersed in fresh DMF (80 °C, 6 h) and then in alcohol (60 °C, 48 h), with the soaking solvent replaced every 12 h to exchange the alcohol. The product was further washed with alcohol (three times) and dried at 80 °C to provide **UiO-68-PT** (3.79 mg) in 80% yield. IR (KBr pellet cm⁻¹): 3338 (m), 2971 (m), 1592 (m), 1417 (s), 1250 (s), 1104 (w), 778 (s), 659 (s). Anal. (%) calcd for the desolvated sample C₂₁₆H₁₅₄N₁₈O₅₆S₆Zr₆: C 60.00, H 3.65, N 5.93, S 4.52; Found: C 59.78, H 3.57, N 6.03, S 4.37.

Synthesis of UiO-68-PTO. **UiO-68-PT** (1 mg) was dispersed in 1 mL of water, and then 10 μL of newly prepared HClO solution (0.1 M) was added; the mixture changed from white to red immediately. After it was centrifuged and washed with water, ethanol, and ether, **UiO-68-PTO** was obtained. IR (KBr pellet cm⁻¹): 3370 (w), 2973 (w), 1588 (s), 1538 (s), 1417 (s), 1249 (w), 1166 (w), 1086 (w), 1045 (w), 1017 (w), 871 (w), 778 (w), 755 (w). Anal. (%) calcd for the desolvated sample C₂₁₆H₁₅₄N₁₈O₅₆S₆Zr₆: C 59.65, H 3.57, N 5.80, S 4.42; Found: C 59.02, H 3.78, N 5.93, S 4.26.

Synthesis of UiO-68-PT'. **UiO-68-PTO** (1 mg) was dispersed in 1 mL of water, and then 50 μL of newly prepared Vitamin C (VC) solution (0.1 M) was added. After it was stirred at room temperature for 30 min, the reaction solution color changed from red to white. After it was centrifuged and washed with water, ethanol, and ether, **UiO-68-PT'** was obtained. IR (KBr pellet cm⁻¹): 3380 (w), 2970 (w), 1588 (s), 1538 (s), 1416 (s), 1250 (w), 1181 (w), 1096 (w), 1018 (w), 826 (w), 778 (w), 753 (w). Anal. (%) calcd for the desolvated sample C₂₁₆H₁₅₄N₁₈O₅₆S₆Zr₆: C 60.00, H 3.65, N 5.93, S 4.52; Found: C 60.21, H 3.76, N 6.12, S 4.49.

MS and ¹H NMR Measurement on the Digested MOFs. In a typical procedure, ~10 mg of activated MOF sample was sonicated in 1 mL of dimethyl sulfoxide and 10 μL of 30% hydrogen fluoride aqueous solution. Thereafter, the system was diluted with H₂O, until no more precipitate formed. The generated organic species was collected by centrifugation, washed with H₂O, and dried in vacuo for MS and ¹H NMR study.

Preparation of MMMs. **UiO-68-PT** (10 mg) were dispersed into an aqueous solution (3 mL) of poly(vinyl alcohol) (40 mg) and then sonicated for 30 min. **UiO-68-PT**-based MMMs were obtained by drying the obtained solution on a flat Teflon mold at 100 °C for 1 h. **H₂L-PT** (10 mg) was dissolved into DMF (1 mL), an aqueous solution (2 mL) of poly(vinyl alcohol) (40 mg) was added, and then the solution was sonicated for 30 min. The **H₂L-PT**-based MMMs were obtained by drying the above solution on a flat Teflon mold at 100 °C for 1 h.

RESULTS AND DISCUSSION

As shown in Scheme 1, the phenothiazine fluorophore with attached $\text{Me}_2\text{L-PT}$ was prepared by Pd-catalyzed Suzuki coupling reaction in DMF under reflux between 4,7-dibromo-substituted and phenothiazine-decorated benzimidazole and 4-(methoxycarbonyl)benzeneboronic acid in moderate yield. After successive alkali hydrolysis and acidification, the obtained $\text{H}_2\text{L-PT}$ was used to synthesize the UiO-68-PT by heating a mixture of $\text{H}_2\text{L-PT}/\text{ZrCl}_4$ in DMF with the aid of acetic acid at 100 °C for 24 h (yield, 80%).

The obtained UiO-68-PT was characterized by scanning electron microscopy (SEM). As indicated in Figure 1a, the

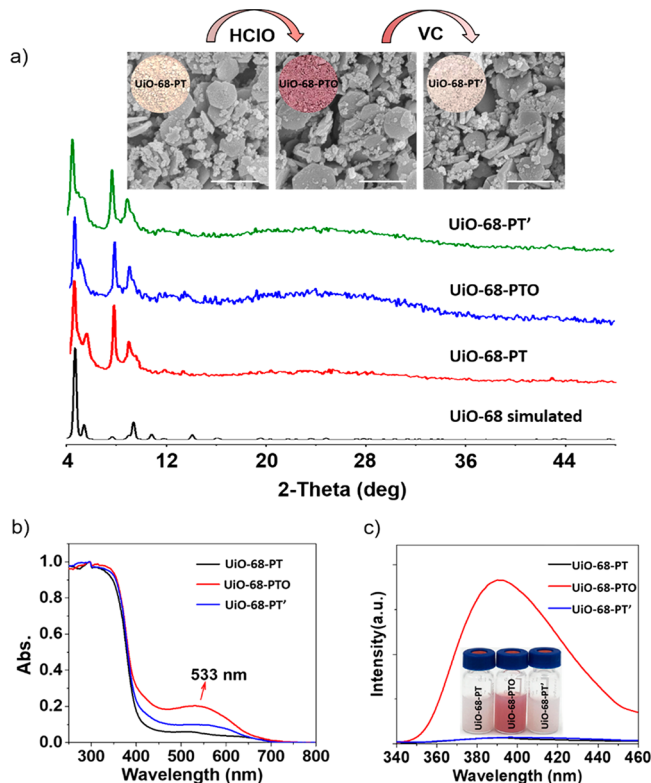


Figure 1. (a) PXRD patterns and photographs (inset, scale bar: 1 μm) of UiO-68-PT , UiO-68-PTO , and $\text{UiO-68-PT}'$. (b) UV-Vis spectra of UiO-68-PT , UiO-68-PTO , and $\text{UiO-68-PT}'$. (c) Fluorescence change of UiO-68-PT (1 mg) in aqueous solution (1 mL) upon successive addition of HClO (0.1 M, 10 μL) and VC (0.1 M, 50 μL) ($\lambda_{\text{ex}} = 323 \text{ nm}$, $\lambda_{\text{em}} = 390 \text{ nm}$). (inset) Photographs of the samples.

obtained UiO-68-PT featured the hexagonal platelike morphology with a diameter of $\sim 700 \text{ nm}$, which was well-supported by the dynamic light scattering (DLS) measurement (Figure S1, Supporting Information). The measured powder X-ray diffraction (PXRD) showed UiO-68-PT has the same crystallographic structure with its pristine UiO-68 ,¹⁶ in which the 2:1 ratio of tetrahedral and octahedral cages formed by the linear organic linkers and 12-connected $\text{Zr}_6\text{O}_4(\text{OH})_4$ nodes were observed. The permanent porosity of UiO-68-PT was explored by measuring nitrogen gas (N_2) adsorption at 77 K. It is different from UiO-68 ; UiO-68-PT herein showed a type-II sorption behavior (Figure S2, Supporting Information). The lack of hysteresis indicated that the adsorption process was reversible and that the adsorption and desorption mechanisms were similar. The measured Brunauer–Emmett–Teller surface

area of UiO-68-PT is only $90.5 \text{ m}^2/\text{g}$, which is significantly smaller than that of UiO-68 ($4170 \text{ m}^2/\text{g}$).¹⁶ The pore sizes in UiO-68-PT are centered at ca. 9.5 and 11.6 Å (Figure S2, Supporting Information), which are also less than its parent UiO-68 (ca. 11.7 and 17.7 Å).¹⁷ Such differences clearly resulted from pore clogging by the phenothiazine-decorated benzimidazole moiety attached to the MOF framework.

Interestingly, the phenothiazine moiety attached UiO-68-PT could go through a white-red-white reversible color change with oxidant HClO and reductant VC successively in aqueous solution. As shown in Figure 1a, after addition of the newly prepared HClO aqueous solution, the white UiO-68-PT changed to deep red UiO-68-PTO immediately. In addition, the deep red color of UiO-68-PTO reverted back to white by the addition of excess VC at room temperature for 5 min, indicating that $\text{UiO-68-PT}'$ was generated. However, the measured PXRD patterns of UiO-68-PT , UiO-68-PTO , and $\text{UiO-68-PT}'$ were identical to that of the UiO-68 , suggesting that their structural integrity and crystallinity were well-preserved during this reversible color change process (Figure 1a). Also, this visual color change was further confirmed by their UV-vis spectra. It is different from white UiO-68-PT and $\text{UiO-68-PT}'$; the deep red UiO-68-PTO showed an intensive absorption band centered at 533 nm (Figure 1b). Besides visual color change, this reversible process was also accompanied by a sharp emission change. As shown in Figure 1c, the luminescence response of UiO-68-PT toward HClO showed that the dramatic emission intensity increase at ca. 390 nm was found to be up to 27-fold after it reacted with HClO. After further addition of reducing agent VC, the strong emission of UiO-68-PTO was quenched again. No obvious differences for particle morphology, permanent porosity, pore widths, and thermogravimetric behavior were observed during this MOF-based redox process (Figure 1 and Figure S2, Supporting Information).

This reversible color change process was further explored by the high-resolution mass spectra (HRMS) based on the digested MOFs by HF. As shown in Figure 2a, the existence of L-PT species in UiO-68-PT was proved by the molecular ion peak (m/z) at 596.1615 (Calcd: 596.1639). In the presence of HClO, the phenothiazine group on UiO-68-PT was oxidized in aqueous solution to afford the phenothiazine sulfoxide containing UiO-68-PTO , which was supported by the molecular ion peak (m/z) observed at 612.1551 (Calcd: 612.1588) (Figure 2b). Moreover, the peak ($m/z = 596.1606$) associated with $\text{H}_2\text{L-PT}$ reappeared after addition of VC, indicating that the $\text{H}_2\text{L-PTO}$ linkage in UiO-68-PTO was reduced and that the UiO-68-PT ($\text{UiO-68-PT}'$) was regenerated in aqueous solution under the given conditions. The ^1H NMR of digested MOFs showed that the $\text{H}_2\text{L-PT}$ could be completely transformed during this process (Figure S3, Supporting Information). In addition, the Fourier transform infrared (FTIR) spectrum of UiO-68-PTO showed that the characteristic band at 1045 cm^{-1} for $>\text{S}=\text{O}$ was observed,¹⁸ which further evidenced the formation of the phenothiazine sulfoxide during this HClO-involved oxidation process (Figure S3, Supporting Information).

Besides visual color change, this reversible redox process also caused a dramatic emission change. As shown in Figure 2d, the strong electron-donating phenothiazine moiety can quench the benzimidazole emission via the photoinduced electron transfer (PET) pathway.¹⁹ With the aid of HClO, the electron-donating phenothiazine was transferred to phenothiazine

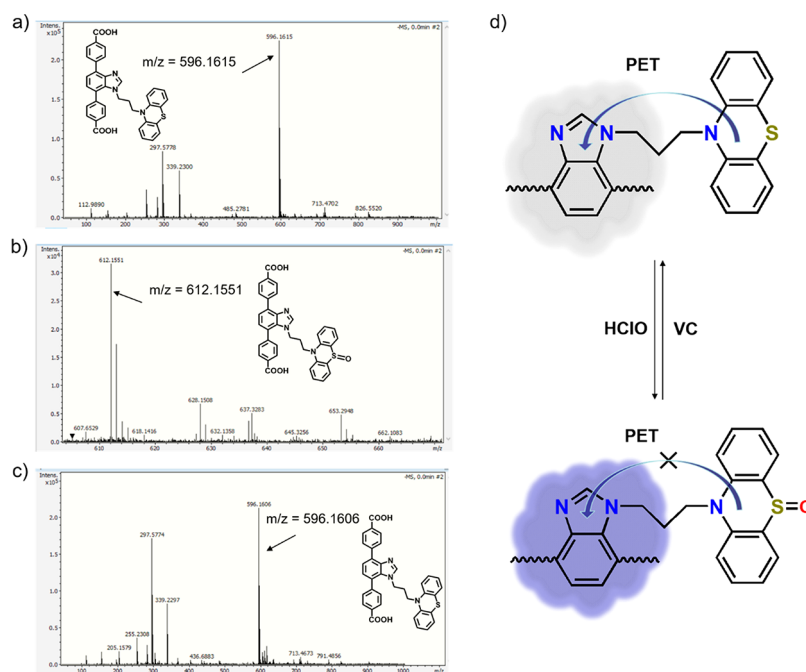


Figure 2. HRMS spectra of the acid-digested UiO-68-PT (a), UiO-68-PTO (b), and UiO-68-PT' (c). The reversible emission change mechanism (d).

sulfoxide, which could significantly prohibit the PET from phenothiazine to benzimidazole; consequently, the benzimidazole-centered strong emission was recovered (Figure 2d). After further reduction of UiO-68-PTO by VC, the phenothiazine-attached UiO-68-PT was regenerated (UiO-68-PT'), and the benzimidazole emission was quenched again.

Furthermore, this MOF-based reversible redox process was also well-supported by the same functional group transformation on the free organic linker of H₂L-PT, and the result demonstrated that the ligand-based redox reaction readily occurred under the same conditions. As shown in the ¹H NMR spectra (Figure S4, Supporting Information), the signals corresponding to the αH and βH on the phenothiazine sulfoxide underwent the clear downfield shift with a Δδ = 1.32 (αH) and 0.63 ppm (βH) after oxidation. Meanwhile, the αH and βH returned to their original positions upon addition of VC.

On the basis of the aforementioned observation, UiO-68-PT could be used as a visual or fluorescent sensor for detecting HClO in aqueous solution. Considering the low HClO concentration in the environment, for example, in tap water, high sensitivity for HClO probe is necessary. For this, the sensitivity of UiO-68-PT was determined by the emission spectra. As indicated in Figure 3a, the emission intensity at 392 nm was linearly related to the HClO concentration in a range from 0 to 80 μM with a linear coefficient up to 0.9947 (Figure S5, Supporting Information). The limit of detection (LOD) was 0.28 μM based on LOD = 3σ/k (where σ = standard deviation, and k = slope of the linear plot).²⁰ Such a low detection limit makes the UiO-68-PT available for detecting HClO in tap water.

Besides sensitivity, the high selectivity is another essential feature for the probe. So, the selectivity of UiO-68-PT toward HClO over other analytes in tap water was examined. As shown in Figure 3b, the color of aqueous solution containing UiO-68-PT (0.1 mg/mL, water) did not show any color

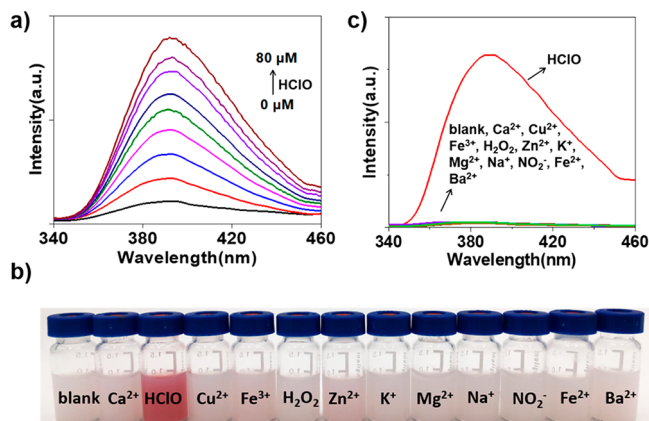


Figure 3. (a) Emission spectra of UiO-68-PT (0.1 mg/mL) upon addition of HClO at different concentrations in the aqueous solution. The emission maximum was observed at 392 nm ($\lambda_{\text{ex}} = 323$ nm). (b) Color change of UiO-68-PT (0.1 mg/mL, water) in the presence of various analytes (0.1 M), from left to right: blank, Ca²⁺, HClO, Cu²⁺, Fe³⁺, H₂O₂, Zn²⁺, K⁺, Mg²⁺, Na⁺, NO₂⁻, Fe²⁺, Ba²⁺. (c) Fluorescence spectra of probe UiO-68-PT (0.1 mg/mL) to HClO (0.1 M) over various relevant species (0.1 M).

change upon addition of each analyte, that is, Ca²⁺, Cu²⁺, Fe³⁺, H₂O₂, Zn²⁺, K⁺, Mg²⁺, Na⁺, NO₂⁻, Fe²⁺, Ba²⁺, which is further confirmed by the emission spectra. As indicated in Figure 3c, only HClO could induce the significant fluorescence increase; no detectable fluorescence changes were observed for other possible species in water. To our delight, the oxidation process of UiO-68-PT by HClO is very quick, and the whole oxidation response time is less than 10 s based on the measured emission intensity (Figure S6, Supporting Information).

For practical application, the UiO-68-PT-based MMM was fabricated. The UiO-68-PT-based MMM (20% content) was readily fabricated by ultrasonically mixing UiO-68-PT (10 mg) and PVA (40 mg) in aqueous solution (3 mL) for 5 min.

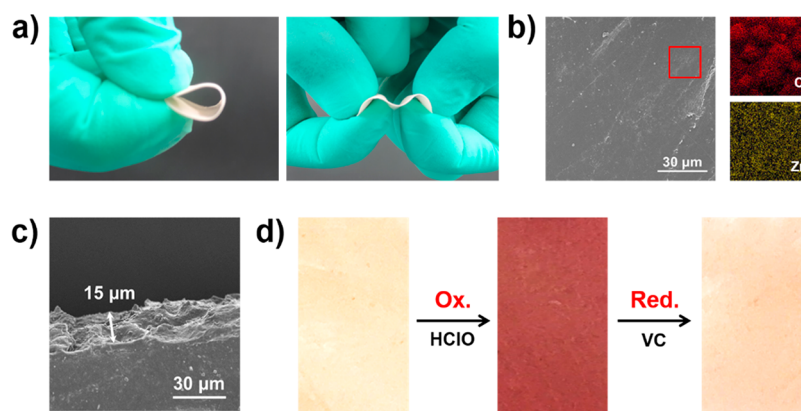


Figure 4. (a) Different views of the UiO-68-PT-based MMM ($1.5 \times 3.0 \text{ cm}^2$) indicating resilience to mechanical stress. (b) SEM image and elemental mapping of the UiO-68-PT-based MMM. (c) SEM image of the cross section of MMM. (d) Color change of the UiO-68-PT-based MMM induced by HClO (5 mg/L) and VC (0.1 M).

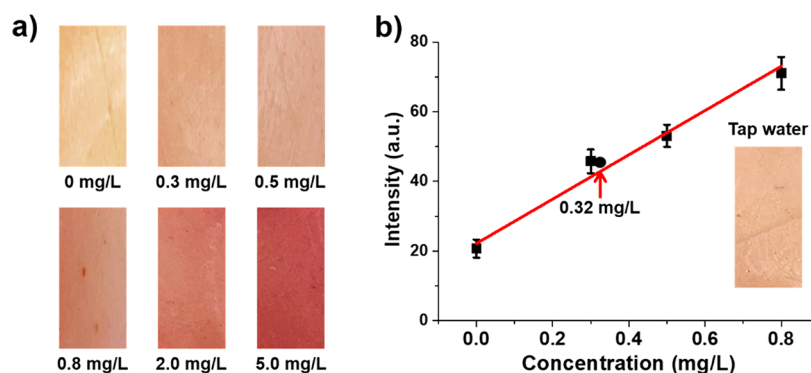


Figure 5. (a) Color change of the UiO-68-PT-based MMM immersed in HClO aqueous solution with different concentrations (<3 min). (b) The linearity between relative intensity and HClO concentration in the range of 0–0.8 mg/L (with the linear coefficient of 0.9801; inset is the test result in tap water).

Afterward, it was dried on the Teflon mold at $100 \text{ }^\circ\text{C}$ for 1 h to afford a stand-alone and elastic membrane with 20 wt % of UiO-68-PT loading (Figure 4a). As shown in Figure 4b, SEM image and elemental mapping showed the obtained free-standing membrane is flat, pliable, and free of macroscopic defects and that the MOF particles were evenly dispersed in the membrane. The cross-sectional image indicated that the membrane is ca. $15 \text{ }\mu\text{m}$ in thickness (Figure 4c). In addition, the membrane surface energy was measured based on the static contact angles (Figure S7, Supporting Information). The drop image was obtained from the drop wetting state (both left and right contact angles) via an image analysis system; meanwhile, the ultrapure water was used as the test liquid, and all the measurements were performed at room temperature. The obtained results showed that the contact angles of PVA and UiO-68-PT-based MMM are $58.5 \pm 2.0^\circ$ and $63.4 \pm 2.0^\circ$, respectively. As expected, the involved MOF particle did not significantly change the hydrophilicity of PVA, which would be beneficial to its application in aqueous media.

After it was immersed in HClO solution (5 mg/L), the light yellow UiO-68-PT-based MMM changed to deep red within 3 min. By addition of VC (0.1 M) at room temperature, the deep red MMM reverted to light yellow (Figure 4d). The MOF structure in the MMM was well-preserved during this color-change process, which was well-supported by the measured PXRD patterns (Figure S8, Supporting Information). Therefore, the UiO-68-PT-based MMM herein could be considered as a reusable colorimetric card for detecting HClO in aqueous

solution under ambient conditions. Although a series of MOF-based MMMs have been reported very recently,²¹ the reversible visual color-changed MOF-MMMs are still unprecedented.²²

As shown in Figure 5a, the visual color change of the UiO-68-PT-based MMM could be clearly observed within a HClO concentration range of 0–5.0 mg/L. Moreover, the relative intensity and HClO concentration showed a good linearity in a range of 0–0.8 mg/L (Figure 5b), which covered the HClO concentration requirement in tap water of China.²³ So, the detection of HClO in tap water was performed. The tap water sample was collected from Jinan (Shandong, China), and it was immediately analyzed after sampling without any pretreatment. After it was immersed in the tap water sample at room temperature for 3 min, the color of the UiO-68-PT-based MMM changed, and the HClO content of 0.32 mg/L was determined based on the intensity–concentration standard curve (Figure 5b). The H₂L-PT-based MMM, however, did not show obvious color changes under the same conditions (Figure S9, Supporting Information).

CONCLUSION

In summary, we report the first of its kind, a novel MOF-based redox-reversible fluorescent probe UiO-68-PT, which was generated from the phenothiazine-decorated benzimidazole bridging dicarboxylic acid ligand and Zr(IV) via in situ one-pot approach. The obtained UiO-68-PT can be a highly sensitive

and selective probe to detect HClO via both visual and fluorogenic observation. More importantly, UiO-68-PT-based MMM was fabricated by mixing MOF with poly(vinyl alcohol), and the obtained MMM can be used as a naked-eye colorimetric card to detect the HClO in tap water. We expect the presented approach to be viable for the fabrication of many new types of MOF-based materials and shaped devices for practical applications, especially for the increasing global environmental issues.

■ ASSOCIATED CONTENT

● Supporting Information

The Supporting Information is available free of charge on the ACS Publications website at DOI: 10.1021/acs.inorgchem.9b01032.

Materials and instrumentation, synthesis of the compound H₂L-PT, N₂ sorption isotherms and pore width of UiO-68-PT, UiO-68-PTO, UiO-68-PT', and MMMs, FTIR spectra, H₂L-PT/H₂L-PTO/H₂L-PT' redox reactions process, water contact angles, and PXRD of PVA and UiO-68-PT-based MMM (PDF)

■ AUTHOR INFORMATION

Corresponding Authors

*E-mail: yananli@sdu.edu.cn. (Y.-A.L.)

*E-mail: yubindong@sdu.edu.cn. (Y.-B.D.)

ORCID

Yan-An Li: 0000-0003-4972-5101

Qun Guan: 0000-0002-5522-5106

Yu-Bin Dong: 0000-0002-9698-8863

Notes

The authors declare no competing financial interest.

■ ACKNOWLEDGMENTS

We are grateful for financial support from NSFC (Grant Nos. 21671122, 21475078, and 21805172), the Taishan Scholar's Construction Project, the Doctoral Fund of Shandong Province (Grant No. ZR2017BB067), and China Postdoctoral Science Foundation funded project (Grant No. 2017M612328).

■ REFERENCES

- (1) (a) Baert, L.; Vandekinderen, I.; Devlieghere, F.; Van Coillie, E.; Debevere, J.; Uyttendaele, M. Efficacy of Sodium Hypochlorite and Peroxyacetic Acid to Reduce Murine Norovirus 1, B40–8, *Listeria* Monocytogenes, and *Escherichia Coli* O157:H7 on Shredded Iceberg Lettuce and in Residual Wash Water. *J. Food Prot.* **2009**, *72*, 1047–1054. (b) Huo, F.-J.; Zhang, J.-J.; Yang, Y.-T.; Chao, J.-B.; Yin, C.-X.; Zhang, Y.-B.; Chen, T.-G. A Fluorescein-Based Highly Specific Colorimetric and Fluorescent Probe for Hypochlorites in Aqueous Solution and Its Application in Tap Water. *Sens. Actuators, B* **2012**, *166*, 44–49.
- (2) Hawkins, C. L.; Davies, M. J. Hypochlorite-induced oxidation of proteins in plasma: formation of chloramines and nitrogen-centred radicals and their role in protein fragmentation. *Biochem. J.* **1999**, *340*, 539–548.
- (3) Daugherty, A.; Dunn, J. L.; Rateri, D. L.; Heinecke, J. W. Myeloperoxidase, a catalyst for lipoprotein oxidation, is expressed in human atherosclerotic lesions. *J. Clin. Invest.* **1994**, *94*, 437–444.
- (4) Yang, Y.; Zhao, Q.; Feng, W.; Li, F. Luminescent Chemosensors for Bioimaging. *Chem. Rev.* **2013**, *113*, 192–270.
- (5) Zhu, H.; Fan, J.; Wang, J.; Mu, H.; Peng, X. An "Enhanced PET"-Based Fluorescent Probe with Ultrasensitivity for Imaging Basal and Elesclomol-Induced HClO in Cancer Cells. *J. Am. Chem. Soc.* **2014**, *136*, 12820–12823.
- (6) Wang, P.; Zhou, F.; Zhang, C.; Yin, S.-Y.; Teng, L.; Chen, L.; Hu, X.-X.; Liu, H.-W.; Yin, X.; Zhang, X.-B. Ultrathin two-dimensional covalent organic framework nanoprobe for interference-resistant two-photon fluorescence bioimaging. *Chem. Sci.* **2018**, *9*, 8402–8408.
- (7) Kenmoku, S.; Urano, Y.; Kojima, H.; Nagano, T. Development of a Highly Specific Rhodamine-Based Fluorescence Probe for Hypochlorous Acid and Its Application to Real-Time Imaging of Phagocytosis. *J. Am. Chem. Soc.* **2007**, *129*, 7313–7318.
- (8) (a) Chen, S.; Lu, J.; Sun, C.; Ma, H. A Highly Specific Ferrocene-Based Fluorescent Probe for Hypochlorous Acid and Its Application to Cell Imaging. *Analyst* **2010**, *135*, 577–582. (b) Chen, X.; Wang, X.; Wang, S.; Shi, W.; Wang, K.; Ma, H. A Highly Selective and Sensitive Fluorescence Probe for the Hypochlorite Anion. *Chem. - Eur. J.* **2008**, *14*, 4719–4724.
- (9) (a) Yuan, L.; Lin, W.; Xie, Y.; Chen, B.; Song, J. Fluorescent Detection of Hypochlorous Acid from Turn-On to FRET-Based Ratiometry by a HOCl-Mediated Cyclization Reaction. *Chem. - Eur. J.* **2012**, *18*, 2700–2706. (b) Xiao, H.; Xin, K.; Dou, H.; Yin, G.; Quan, Y.; Wang, R. A fast-responsive mitochondria-targeted fluorescent probe detecting endogenous hypochlorite in living RAW 264.7 cells and nude mouse. *Chem. Commun.* **2015**, *51*, 1442–1445. (c) Yin, W.; Zhu, H.; Wang, R. A Sensitive and Selective Fluorescence Probe Based Fluorescein for Detection of Hypochlorous Acid and Its Application for Biological Imaging. *Dyes Pigm.* **2014**, *107*, 127–132. (d) Li, J.; Li, P.; Huo, F.; Yin, C.; Liu, T.; Chao, J.; Zhang, Y. Ratiometric Fluorescent Probes for ClO⁻ and in Vivo Applications. *Dyes Pigm.* **2016**, *130*, 209–215.
- (10) Wybraniec, S.; Starzak, K.; Pietrkowski, Z. Chlorination of betacyanins in several hypochlorous acid systems. *J. Agric. Food Chem.* **2016**, *64*, 2865–2874.
- (11) Mei, J.; Hong, Y.; Lam, J. W. Y.; Qin, A.; Tang, Y.; Tang, B. Z. Aggregation-induced emission: the whole is more brilliant than the parts. *Adv. Mater.* **2014**, *26*, 5429–5479.
- (12) (a) Hu, Z.; Deibert, B.; Li, J. Luminescent metal–organic frameworks for chemical sensing and explosive detection. *Chem. Soc. Rev.* **2014**, *43*, 5815–5840. (b) Qiu, S.; Xue, M.; Zhu, G. Metal–organic framework membranes: from synthesis to separation application. *Chem. Soc. Rev.* **2014**, *43*, 6116–6140. (c) Li, F.-L.; Shao, Q.; Huang, X.; Lang, J.-P. Nanoscale Trimetallic Metal–Organic Frameworks Enable Efficient Oxygen Evolution Electrocatalysis. *Angew. Chem., Int. Ed.* **2018**, *57*, 1888–1892. (d) Hu, F.-L.; Mi, Y.; Zhu, C.; Abrahams, B. F.; Braunstein, P.; Lang, J.-P. Stereoselective Solid-State Synthesis of Substituted Cyclobutanes Assisted by Pseudorotaxane-like MOFs. *Angew. Chem., Int. Ed.* **2018**, *57*, 12696–12701. (e) Liu, D.; Lang, J.-P.; Abrahams, B. F. Highly Efficient Separation of a Solid Mixture of Naphthalene and Anthracene by a Reusable Porous Metal–Organic Framework through a Single-Crystal-to-Single-Crystal Transformation. *J. Am. Chem. Soc.* **2011**, *133*, 11042–11045. (f) Liu, D.; Ren, Z.-G.; Li, H.-X.; Lang, J.-P.; Li, N.-Y.; Abrahams, B. F. Single-Crystal-to-Single-Crystal Transformations of Two Three-Dimensional Coordination Polymers through Regioselective [2 + 2] Photodimerization Reactions. *Angew. Chem., Int. Ed.* **2010**, *49*, 4767–4770.
- (13) (a) He, C.; Lu, K.; Lin, W. Nanoscale Metal–Organic Frameworks for Real-Time Intracellular PH Sensing in Live Cells. *J. Am. Chem. Soc.* **2014**, *136*, 12253–12256. (b) Chen, H.; Wang, J.; Shan, D.; Chen, J.; Zhang, S.; Lu, X. Dual-Emitting Fluorescent Metal–Organic Framework Nanocomposites as a Broad-Range PH Sensor for Fluorescence Imaging. *Anal. Chem.* **2018**, *90*, 7056–7063. (c) Xu, R.; Wang, Y.; Duan, X.; Lu, K.; Micheroni, D.; Hu, A.; Lin, W. Nanoscale Metal–Organic Frameworks for Ratiometric Oxygen Sensing in Live Cells. *J. Am. Chem. Soc.* **2016**, *138*, 2158–2161.
- (14) Seoane, B.; Coronas, J.; Gascon, I.; Benavides, M. E.; Karvan, O.; Caro, J.; Kapteijn, F.; Gascon, J. Metal–organic framework based mixed matrix membranes: a solution for highly efficient CO₂ capture. *Chem. Soc. Rev.* **2015**, *44*, 2421–2454.

- (15) (a) Ma, Y.; Xu, G.; Wei, F.; Cen, Y.; Xu, X.; Shi, M.; Cheng, X.; Chai, Y.; Sohail, M.; Hu, Q. One-Pot Synthesis of a Magnetic, Ratiometric Fluorescent Nanoprobe by Encapsulating Fe₃O₄ Magnetic Nanoparticles and Dual-Emissive Rhodamine B Modified Carbon Dots in Metal–Organic Framework for Enhanced HClO Sensing. *ACS Appl. Mater. Interfaces* **2018**, *10*, 20801–20805. (b) Li, Y.-A.; Yang, S.; Li, Q.-Y.; Ma, J.-P.; Zhang, S.; Dong, Y.-B. UiO-68-ol NMOF-Based Fluorescent Sensor for Selective Detection of HClO and Its Application in Bioimaging. *Inorg. Chem.* **2017**, *56*, 13241–13248.
- (16) Cavka, J. H.; Jakobsen, S.; Olsbye, U.; Guillou, N.; Lamberti, C.; Bordiga, S.; Lillerud, K. P. A New Zirconium Inorganic Building Brick Forming Metal Organic Frameworks with Exceptional Stability. *J. Am. Chem. Soc.* **2008**, *130*, 13850–13851.
- (17) (a) Kutzscher, C.; Nickerl, G.; Senkovska, I.; Bon, V.; Kaskel, S. Proline Functionalized UiO-67 and UiO-68 Type Metal–Organic Frameworks Showing Reversed Diastereoselectivity in Aldol Addition Reactions. *Chem. Mater.* **2016**, *28*, 2573–2580. (b) Gómora-Figueroa, A. P.; Mason, J. A.; Gonzalez, M. I.; Bloch, E. D.; Meihaus, K. R. Metal Insertion in a Methylamine-Functionalized Zirconium Metal–Organic Framework for Enhanced Carbon Dioxide Capture. *Inorg. Chem.* **2017**, *56* (8), 4308–4316. (c) Al-Jadir, T. M.; Siperstein, F. R. The Influence of the Pore Size in Metal–Organic Frameworks in Adsorption and Separation of Hydrogen Sulphide: A Molecular Simulation Study. *Microporous Mesoporous Mater.* **2018**, *271*, 160–168.
- (18) Oh, K.-I.; Baiz, C. R. Crowding Stabilizes DMSO–Water Hydrogen-Bonding Interactions. *J. Phys. Chem. B* **2018**, *122*, 5984–5990.
- (19) Liang, L.; Liu, C.; Jiao, X.; Zhao, L.; Zeng, X. A Highly Selective and Sensitive Photoinduced Electron Transfer (PET) Based HOCl Fluorescent Probe in Water and Its Endogenous Imaging in Living Cells. *Chem. Commun.* **2016**, *52*, 7982–7985.
- (20) Radford-Knoery, J.; Cutter, G. A. Determination of Carbonyl Sulfide and Hydrogen Sulfide Species in Natural Waters Using Specialized Collection Procedures and Gas Chromatography with Flame Photometric Detection. *Anal. Chem.* **1993**, *65*, 976–982.
- (21) (a) Lin, R.; Villacorta Hernandez, B.; Ge, L.; Zhu, Z. Metal Organic Framework Based Mixed Matrix Membranes: An Overview on Filler/Polymer Interfaces. *J. Mater. Chem. A* **2018**, *6*, 293–312. (b) Ghalei, B.; Sakurai, K.; Kinoshita, Y.; Wakimoto, K.; Isfahani, A. P.; Song, Q.; Doitomi, K.; Furukawa, S.; Hirao, H.; Kusuda, H.; Kitagawa, S.; Sivaniah, E. Enhanced Selectivity in Mixed Matrix Membranes for CO₂ Capture through Efficient Dispersion of Amine-Functionalized MOF Nanoparticles. *Nat. Energy* **2017**, *2*, 17086. (c) Katayama, Y.; Bentz, K. C.; Cohen, S. M. Defect-Free MOF-Based Mixed-Matrix Membranes Obtained by Corona Cross-Linking. *ACS Appl. Mater. Interfaces* **2019**, *11*, 13029. (d) Zhang, Y.; Feng, X.; Li, H.; Chen, Y.; Zhao, J.; Wang, S.; Wang, L.; Wang, B. Photoinduced Postsynthetic Polymerization of a Metal–Organic Framework toward a Flexible Stand-Alone Membrane. *Angew. Chem., Int. Ed.* **2015**, *54*, 4259–4263. (e) Mao, Y.; Li, J.; Cao, W.; Ying, Y.; Hu, P.; Liu, Y.; Sun, L.; Wang, H.; Jin, C.; Peng, X. General Incorporation of Diverse Components inside Metal–Organic Framework Thin Films at Room Temperature. *Nat. Commun.* **2014**, *5*, 5532. (f) Yao, B.-J.; Jiang, W.-L.; Dong, Y.; Liu, Z.-X.; Dong, Y.-B. Post-Synthetic Polymerization of UiO-66-NH₂ Nanoparticles and Polyurethane Oligomer toward Stand-Alone Membrane for Dyes Removal and Separation. *Chem. - Eur. J.* **2016**, *22*, 10565–10571. (g) Jiang, W.-L.; Ding, L.-G.; Yao, B.-J.; Wang, J.-C.; Chen, G.-J.; Ma, J.-P.; Ji, J.; Dong, Y.; Dong, Y.-B.; et al. A MOF-membrane based on covalent bonding driven assembly of NMOF with organic oligomer and its application for membrane reactor. *Chem. Commun.* **2016**, *52*, 13564–13567. (h) Yao, B.-J.; Ding, L.-G.; Li, F.; Li, J.-T.; Fu, Q.-J.; Ban, Y.-J.; Guo, A.; Dong, Y.-B. Chemical Cross-linked MOF membrane Generated from Imidazolium-Based Ionic Liquid Decorated UiO-66 Type NMOF and its Application toward CO₂ Separation and Conversion. *ACS Appl. Mater. Interfaces* **2017**, *9*, 38919–38930.
- (22) (a) Zhao, C.-W.; Ma, J.-P.; Liu, Q.-K.; Wang, X.-R.; Liu, Y.; Yang, J.; Yang, J.-S.; Dong, Y.-B. An in Situ Self-Assembled Cu₄I₄-MOF-Based Mixed Matrix Membrane: A Highly Sensitive and Selective Naked-Eye Sensor for Gaseous HCl. *Chem. Commun.* **2016**, *52*, 5238–5241. (b) Zhang, X.; Zhang, Q.; Yue, D.; Zhang, J.; Wang, J.; Li, B.; Yang, Y.; Cui, Y.; Qian, G. Flexible Metal–Organic Framework-Based Mixed-Matrix Membranes: A New Platform for H₂S Sensors. *Small* **2018**, *14*, 1801563.
- (23) GB5749-2006 of Standardization Administration of the People's Republic of China.